

HAP1 is an in vivo UBE3A target that augments autophagy in a mouse model of Angelman syndrome

Tingting Wang^a, Jingyu Wang^a, Jie Wang^{b,c}, Lin Mao^a, Bin Tang^a, Peter W. Vanderklish^d, Xun Liao^e, Zhi-Qi Xiong^{b,c}, Lujian Liao^{a,*}

^a Shanghai Key Laboratory of Regulatory Biology, Key Laboratory of Brain Functional Genomics of Ministry of Education, School of Life Sciences, East China Normal University, Shanghai 200241, China

^b Institute of Neuroscience, State Key Laboratory of Neuroscience, CAS Center for Excellence in Brain Science and Intelligence Technology, Shanghai Institutes for Biological Sciences, Chinese Academy of Sciences, Shanghai 200031, China

^c University of Chinese Academy of Sciences, Beijing 100049, China

^d Department of Molecular Medicine, Scripps Research, 10550 North Torrey Pines Road, La Jolla, CA 92037, United States

^e Chengdu Institute of Biology, Chinese Academy of Sciences, Chengdu 610041, China



ARTICLE INFO

Keywords:

UBE3A
HAP1
Angelman syndrome
autophagy
SILAM
Proteome

ABSTRACT

Angelman syndrome (AS) is a severe neurodevelopmental disorder caused by maternal mutation and paternal imprinting of the gene encoding UBE3A, an E3 ubiquitin ligase. Although several potential target proteins of UBE3A have been reported, how these proteins regulate neuronal development remains unclear. We performed a large-scale quantitative proteomic analysis using stable-isotope labeling of amino acids in mammals (SILAM) in mice with maternal *Ube3a* mutation. We identified huntingtin (Htt)-associated protein (HAP1), a protein that is involved in Huntington's disease (HD), as a new target of UBE3A. We demonstrate that HAP1 regulates autophagy at the initiation stage by promoting PtdIns3K complex formation and enhancing its activity. HAP1 also co-localized with MAP1LC3 (LC3) and other proteins involved in autophagosome expansion. As a result, HAP1 increased autophagy flux. Strikingly, knocking down of HAP1 alleviated aberrant autophagy in primary neurons from AS mice. Concordantly, treatment of AS neurons with an autophagy inhibitor alleviated the reduction in density of dendritic spines. Furthermore, autophagy inhibition in AS mice partially alleviated a social interaction deficit as shown in open field test. Thus, our results identify HAP1 as an in vivo UBE3A target that contributes to deregulated autophagy and synaptic dysfunction in the central nervous system of AS mouse.

1. Introduction

Angelman syndrome (AS) is a neurodevelopmental disorder characterized by cognitive disability, motor dysfunction, hyperactivity, speech impairment, variable autism spectrum behaviors and frequent seizures (Kishino et al., 1997; Mabb et al., 2011). The disorder is caused by disruption of the maternally expressed and paternally imprinted gene *Ube3a* (also known as E6AP), which encodes a HECT domain E3 ubiquitin ligase that targets substrate proteins, including itself, for proteasomal degradation (de Bie and Ciechanover, 2011). While UBE3A insufficiency causes AS, duplication or triplication of UBE3A is linked to Autism, indicating that the E3 ligase plays a pivotal role in brain development (Glessner et al., 2009; Kishino et al., 1997). For this reason, efforts have been made to identify its substrates in order to understand the pathogenesis of AS. Studies focusing on particular UBE3A

complexes and pathways have identified p53, HERC2, Ephexin5 and other proteins as direct targets (Kühnle et al., 2011; Margolis et al., 2010; Martinez-Zapien et al., 2016). Arc, an activity-regulated cytoskeletal protein that regulates synaptic AMPA receptor levels, was identified as an indirect target of UBE3A (Greer et al., 2010; Kühnle et al., 2013; Pastuzyn and Shepherd, 2017), with altered expression in AS mice leading to impaired homeostatic plasticity. However, the set of UBE3A substrates in brain is largely unknown, and may be sizeable in light of recent data from an orthogonal ubiquitin transfer method applied in cell culture (Wang et al., 2017), which found 130 direct targets. Moreover, there is a paucity of information on how UBE3A-related proteome changes in AS give rise to neurodevelopmental phenotypes of the syndrome, such as reduced synaptic density. Since the loss of UBE3A predominantly causes abnormalities in the central nervous system, in vivo target profiling using brain tissues stands the best

* Corresponding author.

E-mail addresses: liaoxun@cib.ac.cn, xiongzhiqu@ion.ac.cn, ljliao@bio.ecnu.edu (L. Liao).

chance of identifying phenotypically relevant molecular abnormalities in AS.

Postnatal synaptic development is a dynamic process involving the elaboration and activity dependent pruning of synapses, in which autophagy plays a pivotal role (Tang et al., 2014). Autophagy is an evolutionarily conserved process to deliver cytosolic protein aggregates or damaged organelles for lysosomal degradation, and abnormal autophagy is implicated in many diseases including neurological disorders (Li et al., 2014). Insufficient or excessive autophagy may perturb the homeostasis and normal functions of synaptic connections (Yang et al., 2013). In mouse models of the autism spectrum disorders (ASD), tuberous sclerosis and fragile X syndrome (FXS), impairments in autophagy downstream of exaggerated mTOR activity have been mechanistically linked to increased dendritic spine density and changes in spine morphology (Yan et al., 2018); changes in spine density appear to be due to reduced synaptic pruning (Tang et al., 2014). Similarly, insufficient autophagy due to ATG7 mutation was recently shown to result in increased dendritic spine density in dopaminergic neurons (Su et al., 2017). Previous studies have revealed that UBE3A localizes to synapses and that AS mice exhibit reduced dendritic spine density and an increased proportion of immature spines in hippocampus (Dindot et al., 2008; Margolis et al., 2010). Such observations raise the possibility that reduced dendritic spine density in AS stems from increased autophagic flux.

To define a broader set of potential UBE3A targets and related proteome changes, we performed large-scale quantitative proteomic analysis using stable-isotope labeling of amino acids in mammals (SILAM) in three brain regions from AS mice: cortex, hippocampus, and cerebellum. From the altered proteins we noted the increase of the autophagy regulator Huntington-associated protein 1 (HAP1) in AS mice. HAP1 is a brain-enriched adaptor protein for huntingtin (Gutekunst et al., 1998; Li et al., 1995), complexes of which enhance autophagosome transport (Wong and Holzbaur, 2014). HAP1 interacts with KIF5 and dynactin p150 (Li et al., 1998; Twelvetrees et al., 2010), suggesting that it regulates intracellular transport and sorting of protein-containing membrane vesicles to lysosomes and other compartments (Engelender et al., 1997; Hirokawa, 1998; Li et al., 1998). We hypothesized that increased HAP1 in AS promotes autophagic flux by transporting autophagosomes to lysosomes for fusion, and leading to altered synaptic development. Our data support HAP1-mediated enhancement of autophagy flux, and rather surprisingly, we found that increased HAP1 facilitated the initiation of autophagy through interacting with the Beclin1 (BECN1)-ATG14-PIK3C3 (VPS34) complex, resulting in increased PtdIns3K activity. Increased autophagy correlated with abnormal dendritic spine morphology, which was partially rescued by inhibiting autophagy. These findings shed new light on the origins of synaptic dysfunction in AS and suggest that therapeutic targets for the syndrome may be found within autophagic signaling pathways.

2. Materials and methods

2.1. Animals

All animal experiments were performed following the Institutional Animal Care and Use Committee protocols from East China Normal University (ECNU). AS (*Ube3a*^{m−/p+}) mice were kindly provided by Dr. Zhiqi Xiong, Chinese Academy of Sciences, Shanghai.

2.2. Behavior

Mice were administered with HCQ (20 mg/kg) via intraperitoneal injection every 2 days from P14 and lasted for two weeks, with PBS as the control. Behavioral tests were performed by an experimenter blind to the genotype and drug treatment. Mice were acclimated to the test room for 20 min before each behavior test. Starting from P30, open

field test was performed on day 1, rotarod test was performed on day 2 to day 5, and the fear condition test was performed on day 6 to day 9. For the open field test, each mouse was placed in a brightly, open-field arena (40 × 40 × 30 cm) and were allowed to explore for 15 min. The acquired raw data was analyzed with ANY-maze software. For rotarod test, mice were placed on an accelerating 3-cm-diameter rotating rod for three trials. Mice from each group were trained for adaptation at the first day at 5 rpm/min, and then increased speed at the subsequent two days up to 25 rpm/min with constant acceleration. The mean latency to fall during the three trials was recorded. For contextual fear conditioning, each mouse was placed in a test chamber on the training day. After 5 min of free exploration (pre-shock freezing), the mouse received an auditory tone (2000 Hz, 80 db, 30 s) followed by a foot-shock (0.7 mA, 2 s). The training was repeated once for two days and was remained in the chamber for 1 min. Twenty-four hours after training, mice were returned to the same test chamber for 5 min and tested for freezing in response to the training context (contextual freezing). Then, the environmental settings of the test chamber were altered and the mice were placed back in the modified chamber. The mice were allowed 3 min of free exploration, and then the auditory tone (80 db, 3 min) was presented to test the fear response to the cue (cued freezing).

2.3. Cell culture, transfection and protein expression

HeLa, HEK293T, and Neuro2A cells were cultured in Dulbecco's modified Eagle's medium (DMEM) supplemented with 10% fetal bovine serum, penicillin/streptomycin in a 5% CO₂ incubator at 37 °C. For starvation treatment, cells were washed with PBS and incubated in glucose-free DMEM without serum. Transfection was conducted by Lipofectamine 2000 or polyethylenimine (PEI), and samples were collected 48 h after transfection. Primary cortical or hippocampal neurons were prepared using standardized method. Specifically, brain tissues from embryonic D18 fetus were dissociated by incubation in papain. Neurons were cultured in Neurobasal medium (Invitrogen, 10,888,022) supplemented with B27 (Invitrogen, 17,504,044) and were fed every third day by replacing half of the medium with fresh medium.

2.4. Immunoprecipitation, immunoblotting

Cell lysates were prepared in buffer containing 50 mM Tris-HCl (pH 7.5), 150 mM NaCl, 1 mM EDTA, 1% Triton X-100, 1 mM PMSF, 1 mM Na₃VO₄, and protease inhibitor cocktail (Sigma). The lysates were clarified by centrifugation at 12,000 rpm and were subjected to immunoprecipitation using specific antibodies conjugated onto agarose beads. Precipitated complexes were washed three times with binding buffer, and were boiled in loading buffer before western blot analysis.

2.5. Immunofluorescence and immunohistochemistry

Cells grown on coverslips were washed with PBS twice, and then fixed in 4% paraformaldehyde for 20 min at RT. Fixed cells were permeabilized with 0.5% Triton X-100 in PBS for 10 min on ice, blocked with 5% bovine serum albumin in PBS for one hour, and incubated with primary antibodies at 4 °C overnight. After washing three times with PBS, cells were incubated with Alexa Fluor 488-conjugated, Alexa Fluor 564-conjugated, or Alexa Fluor 405-conjugated anti-rat, anti-rabbit, or anti-mouse secondary IgG antibodies (Invitrogen) for 1 h for labeling of distinct proteins. All the images were acquired on a laser confocal microscope (Leica TCS442 SP5) using 63× or 100× oil-immersion objective lens.

AS or wild type mice were fixed by cardiac perfusion with 4% paraformaldehyde. Then, the brains were dissected and fixed in 4% paraformaldehyde at 4 °C overnight, dehydrated for 1 day with 20% sucrose in PBS and 1 day with 30% sucrose sequentially, embedded in Optimal Cutting Temperature compound (SAKURA), sectioned at 12 µm

by freezing microtome. Primary antibodies were incubated at 4 °C overnight after blocking with 5% BSA, followed by diaminobenzidine staining following manufacturer's instructions.

2.6. Statistical analysis

Unpaired Student's *t*-test assuming two-tailed distribution was applied to calculate statistical significance. All results were presented as average SD (standard deviation) from at least triplicate experiments. *, **, and *** represents $P < .05$, $P < .01$, and $P < .001$, respectively. The symbol "ns" stands for non-significant.

2.7. Chemical reagents, antibodies and plasmids

Chloroquine (C6628), hydroxychloroquine (90527), and MG132 (C2211) were purchased from Sigma. The following antibodies were used in immunoblotting and immunofluorescent staining experiments. Flag (1:5000, Sigma, F1804), β-Actin (1:5000, YEASEN, 30101-ES10, CHN), UBE3A (1:1000, Sigma, U3884), HAP1 (1:500, BD Biosciences, 611,302), Ubiquitin (1:500, Abcam, ab7780), LAMP1 (1:100, Santa Cruz Biotechnology, sc-19,992), p62/SQSTM1(1:2000, Sigma, P0067), LC3 (1:2000, Sigma, L7543), NeuN(1:500, Millipore MAB377), ATG14 (1:1000, CST #96752), p- BECN1 (S93), BECN1, VPS34, were kindly gifts from Dr. Yan Chen (Chinese Academy of Sciences, Shanghai).

2.8. Quantitative real-time PCR

Total RNA was isolated from mouse brain or HEK293T cells using RNeasy Mini Kit (Qiagen). Isolated RNA (1 μg) was reverse-transcribed using Oligo (dt) primer (Takara). Quantitative real-time PCR was performed using the SYBR Green Master Mix (Promega). The housekeeping gene GAPDH was used as the internal control. The primers were as follows: mHAP1 (5'- CTGAGGAGCTCGAACATCT-3' and 5'- GTGGCA TCGCCCTCTGCTC-3'), mGAPDH (5'-CATGCCCTCCGTGTCCTA-3' and 5'-CCTGCTTACCAACCTTCTTGAT-3'), the experimental procedure was as previously described (Tang et al., 2015).

2.9. Spine morphology

Cortical or hippocampal neurons were infected with GFP lentiviral system at DIV13, and experiments were carried out at DIV16. Cells grown on coverslips were washed with PBS for three times, then fixed in 4% paraformaldehyde for 20 min at RT and mounted on glass slides for confocal imaging. Z-stack was applied to capture spines from various layers. More than fifteen cells were collected for statistical analysis, and the spine density or maturation condition of each group was measured according to previously described protocol (Dindot et al., 2008; Yi et al., 2015).

2.10. Ni-NTA pulldown assay

HEK293T cells were transfected with HA-tagged HAP1 together with Flag-tag UBE3A or His-Ubiquitin. After 48 h, cells were washed with PBS and harvested in Buffer A (containing 28.6 g guanidine hydrochloride, 23.29 ml 0.2 M Na₂HPO₄, 1.3 ml 0.2 M NaH₂PO₄, 0.5 ml 1 M Tris-HCl (pH 8.0), 35 μl β-mercaptoethanol in 50 ml total volume). After lysing for 30 min at RT, Ni-NTA beads were added and incubated for 6 h at RT followed by washing with buffer B (12 g Urea, 11.8 ml 0.2 M Na₂HPO₄, 0.7 ml 0.2 M NaH₂PO₄, 0.25 ml 1 M Tris-HCl (pH 8.0), 17.5 μl β-mercaptoethanol in 25 ml total volume) and buffer C (12 g Urea, 2.81 ml 0.2 M Na₂HPO₄, 9.68 ml 0.2 M NaH₂PO₄, 0.25 ml 1 M Tris-HCl (pH 8.0), 17.5 μl β-mercaptoethanol in 25 ml total volume). Finally, the beads were eluted with Elution buffer (681 mg imidazole, 7.5 ml 1 M Tris-HCl (pH 6.7), 30% glycerol (vol/vol), 2.5 g SDS, 2.52 ml β-mercaptoethanol in a 50 ml total volume), and then boiled with protein loading buffer for Western blot analysis.

2.11. SiRNA and transfection

The sequences used for siRNA knock down were as follows (5'-3'), siHAP11#- GCUCCUACAUGCAGGAUATT, siHAP12#-GAAGUAUGU CCUCAGCAATT. The scrambled siRNA sequence, Scrbl-UUCUCCGA ACGUGUCACGUUTT. Primary neurons were transfected with siRNAs at DIV 12 with lipo3000 according to manufacturer's description. Two days after transfection, the cells were lysed in RIPA buffer, and the protein extraction and concentration assay were performed.

2.12. LC-MS/MS and data analysis

For SILAM experiments, WT mice were labeled with 13C6-Lys, while the AS mice were non-labeled with normal food. The brain was dissected into cortex, cerebellum and hippocampus. Briefly, the brain regions were homogenized with tissue homogenizer in lysis buffer (7 M urea, 2 M thiourea in 50 mM Tris-HCl (pH 8.0), 150 mM NaCl, 1 mM EDTA with protease inhibitor Cocktail tablets, PMSF, NaF, Na₃VO₄), the brain lysates were sonicated followed by centrifuging at 14000 rpm. After determining protein concentration using Bradford assay kit, 1 mg of protein from each sample was taken for reduction with DTT (10 mM) at 55 °C for 30 min, then alkylation with chloroacetamide (15 mM) in the dark for 30 min. Ten microgram of protein was used to determine labeling efficiency. Then, equal amount of labeled (WT) and unlabeled (AS) lysates were combined as a mixture of 2 mg total protein. Afterwards, the protein lysates were diluted to 2 M Urea concentration with 50 mM Tris-HCl (pH 8.0) for trypsin digestion overnight in a 1:50 enzyme-to-substrate ratio, the digestion reaction were stopped with trifluoroacetic acid (TFA) and desaltsed by reversed-phase C18 Sep-Pak SPE cartridge (Millipore, USA). The desalted peptides were fractionated offline using basic pH reversed-phase (bRP) chromatography into 60 fractions and then combined to 12 final fractions. The pooled fractions were dried completely using vacuum centrifugation and desaltsed. The resulting peptides were analyzed on an Easy-nLC1000 LC system (Thermo Scientific) coupled to a Q-Exactive mass spectrometer with in-house packed C18 column, the mass spectrometry was operated by acquiring an MS1 scan ($R = 70,000$) followed by 12 MS/MS scans ($R = 17,500$), and the HCD collision energy was set to 27. Raw files were processed in the MaxQuant software environment (version 1.5.3.8) and searched against the Uniprot Mouse Database (Proteome ID: UP1000000589).

2.13. Bioinformatics analysis

Principal components analysis (PCA) were performed in R. For functional annotation, the significant changed proteins were selected by MAD analysis using a Z score cutoff value of 2.0. Then the changed proteins were analyzed with the DAVID bioinformatics resource v6.7 (<https://david.ncifcrf.gov/>). The gene ontology terms of biological process (GOBP), molecular function (GOMF) and cellular component (GOCC) were analyzed and top ten enriched terms were displayed.

3. Results

3.1. SILAM-based quantitative mass spectrometry identifies UBE3A targets in mouse brain

We verified the dramatically reduced expression of UBE3A in AS mouse by western blot (Fig. 1A). We then applied a quantitative mass spectrometry approach based on stable-isotope labeling of amino acids in mammals (SILAM) to explore proteome changes. This approach captures protein expression changes resulting from UBE3A insufficiency on proteostasis at any level. The experiment involves comparing proteome expression in three brain regions between wild type (WT) and AS mice at postnatal day 14 (Fig. S1A). WT mice were labeled for at least 14 weeks to reach 97% ¹³C6-Lys labeling efficiency (Fig. S1B). To

increase the quantitative depth, we performed off-line fractionation using basic reversed-phase (bRP) chromatography. In total, we quantified 3200 proteins in all brain regions (Fig. 1B, Fig. S1A). Overall, we achieved a mass measurement error within 10 ppm (Fig. S1C). The

UBE3A protein itself was identified and its expression was four-fold lower in AS mouse brain (Fig. 1C). In addition, the quantification consistency between the two biological replicates was high, as depicted by Pearson's correlation analysis (Fig. S1D). Principal components

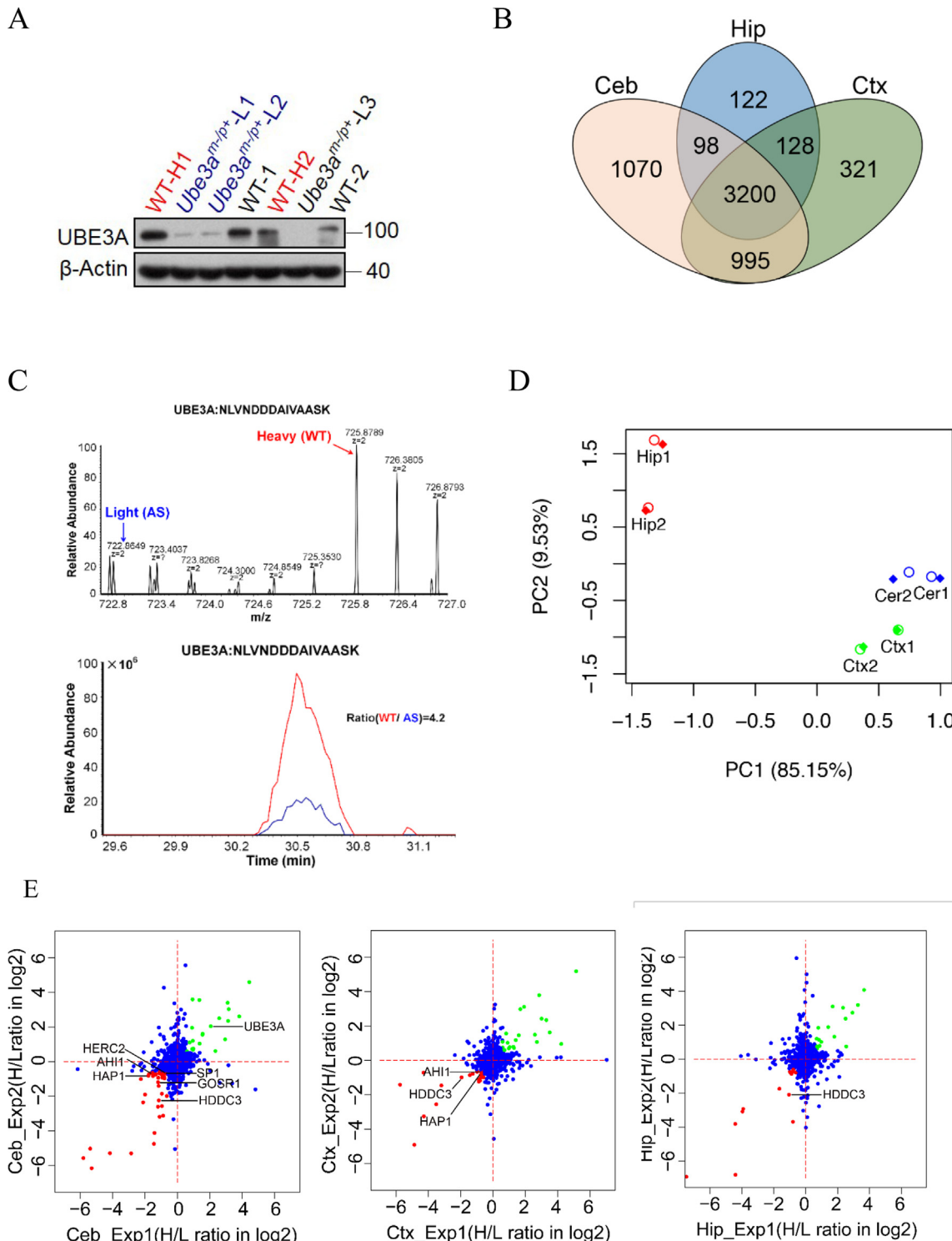


Fig. 1. SILAM-based quantitative mass spectrometry identifies UBE3A targets in mouse brain. (A) Western blot analysis of brain tissues from wild type and AS mice used in SILAC experiments using an antibody against UBE3A. Among them, WT-H1 and WT-H2 mice were fed with heavy food, *Ube3a^{m-p+}-L1* and *Ube3a^{m-p+}-L2* were fed with light food. The other mice were not taken for the proteomic experiment, *Ube3a^{m-p+}-L3* was also labeled, WT-1 and WT-2 were fed in normal food. (B) Venn Diagram shows the number of quantified proteins in three brain regions (Ceb: cerebellum, Hip: hippocampus, Ctx: cortex). (C) MS1 spectra and reconstructed chromatograms of a unique peptide of UBE3A. (D) Principal components analysis (PCA) of the three brain regions based on protein intensity, shown are the first and the second components. (E) Correlation plots of two biological repeats showing the up- or down regulated proteins identified by median absolute deviation (MAD) analysis.

analysis (PCA) of protein intensities showed that proteins in hippocampus distributed away from cortex and cerebellum, whereas the proteins from heavy (WT, solid shape) and light (AS, open shape) samples tightly clustered together (Fig. 1D), suggesting that loss of UBE3A did not cause global changes in protein expression. To identify differentially expressed proteins, we applied a median absolute deviation (MAD) analysis integrating a fold change cutoff value of 1.5 and a Z score cutoff value of 2.0. As represented in scatter plots of proteins quantified in each brain region (Fig. 1E), we identified 168 up- (red) and down-regulated (green) proteins (Table S1). Among these proteins are several known UBE3A targets including HERC2 and RAD23A (Fig. 1E and Table S1). In addition, we found potential new targets such as HAP1, GOSR1, AHI1, which participate in protein transport as revealed by gene ontology analysis (Fig. S1E). Gene ontology analysis in the category of molecular function also indicated that over 50 proteins were enriched in protein binding process, which implied that protein-protein interaction might play a crucial role in the pathogenesis of AS.

3.2. UBE3A interacts with and promotes the ubiquitination of HAP1

To validate potential targets, we performed co-expression experiments in HEK293T cells. When co-expressed with UBE3A, except for HDDC3, levels of TRAF3, AHI1, GOSR1, SP1 and CaMK2c were greatly reduced by UBE3A in a dose-dependent manner, supporting our proteomic results. The expression levels of these proteins increased to normal by treatment with the proteasome inhibitor MG132, suggesting that UBE3A mediated proteasome-dependent degradation of these targets (Fig. S2A). Among the verified targets, we focused on HAP1 because of its involvement in nervous system development and vesicle transport, a process that might be linked to the pathogenesis of AS. The precursor ion spectra and reconstructed chromatograms of HAP1 peptide show highly elevated levels in AS mouse brain (Fig. S2B). The mass spectrometry results were confirmed by western blot analysis of brain tissues using an antibody against endogenous HAP1 (Fig. 2A, Fig. S2C-E), which revealed an approximately 40% increase in AS mice. HAP1 expression was reduced in a dose-dependent manner by co-expressing UBE3A, an effect that was blocked by treatment with MG132 or Bortezomib (Fig. 2B). Co-expression with a ligase-dead (UBE3A-LD, C838A mutant) form of UBE3A had no effect on HAP1 expression (Fig. 2B). Meanwhile, Real-time PCR revealed that HAP1 mRNA expression was not different between WT and AS brain or in HEK293T cells (Fig. S2F-G), ruling out that UBE3A regulates HAP1 expression at protein level. Western blot analysis of WT mouse cerebellum revealed that HAP1 expression peaks early between postnatal days P1-P7 and declines substantially with age thereafter until P45 (Fig. S2H), this observation was consistent with a previous study (Xiang et al., 2015). In AS mice, however, HAP1 maintained an abnormally high expression level in the cerebellum even at P45 (Fig. S2E), which suggested that accumulated HAP1 was an important pathogenic factor in AS mouse.

We confirmed that UBE3A interacts with HAP1 in P14 brain lysates using co-immunoprecipitation (Fig. 2C). In HEK293T cells co-transfected with HA-tagged HAP1 and Flag-tagged UBE3A, the two proteins were mutually co-precipitated (Fig. 2D), suggesting a physical interaction between the two proteins. Since UBE3A is an ubiquitin ligase, we asked whether the interaction led to HAP1 degradation. Co-expression of UBE3A in cells resulted in reduced half-life of HAP1. In contrast, co-expression of ligase-dead UBE3A maintained a longer HAP1 half-life (Fig. 2E-F). Thus, UBE3A controls the stability of HAP1 in a ligase-dependent manner.

We then tested whether HAP1 is a UBE3A target. Using in vivo ubiquitination assay in HEK293T cells, we found that wild type UBE3A dramatically promoted HAP1 ubiquitination, while the ligase-dead UBE3A led to a much weaker HAP1 ubiquitination (Fig. 2G), indicating that UBE3A could be at least one of the E3 ligase for HAP1. To identify the ubiquitination sites of HAP1, we co-transfected his-tagged wild type or a lysine only (at residue 48) ubiquitin mutant with HAP1 and UBE3A

in HEK293T cells. We enriched the ubiquitin-conjugated species with Ni-NTA followed by mass spectrometry analysis and identified three ubiquitination sites on HAP1 (Fig. S3B). Two ubiquitination sites are located at the N-terminal, while the third one is at the C-terminal (Fig. S3A). We constructed HAP1 mutants in which the lysine residues were replaced with arginine (HAP1-2KR, 3KR), and co-expressed these plasmids with UBE3A. Western blot analysis showed that HAP1 with 3KR mutation was more resistant to UBE3A-mediated degradation (Fig. S3C). Moreover, ubiquitination of HAP1 decreased in AS brain (Fig. 2H), consistent with the reduced ligase activity of UBE3A.

3.3. Autophagy is elevated in AS neurons

HAP1 plays a pivotal role in vesicle trafficking (Rong et al., 2007), and a few studies suggested that it also plays a role regulating autophagy (Mejia et al., 2013; Wong and Holzbaur, 2014). We hypothesized accordingly that abnormally increased expression of HAP1 in AS neurons resulted in deregulated autophagy. We monitored LC3 and SQSTM1/p62, two essential autophagy markers, in primary cortical neurons. In AS neurons the basal LC3II level was increased, while p62 showed clear reduction (Fig. 3A-B). Immunofluorescent labeling of p62 further supported these observations, p62 puncta were reduced in AS neurons at 10 days in vitro (DIV10) (Fig. 3C). Furthermore, immunohistochemistry analysis of P14 cortices showed reduced p62 staining in AS mice, suggesting excessive autophagic degradation (Fig. 3D). *Ube3a* is specifically imprinted in neurons, we detected the expression of p62 in NeuN positive cells, where reduced p62 staining was also verified in AS in P14 cortices (Fig. 3E). These observations suggested that there is elevated basal autophagic activity in AS neurons.

3.4. HAP1 enhances basal autophagy

To test whether increased autophagy activity is due to HAP1 up regulation, we over expressed HAP1 in HeLa cells and observed a slightly increased LC3II level at basal condition (Fig. 4A). Consistently, over expression of HAP1 increased GFP-LC3 puncta formation that partially co-localized with HAP1 (Fig. 4B). Furthermore, we found that some HAP1 co-localized with LC3 as well as with LAMP1, a lysosome marker (Fig. 4C). Statistical analysis of confocal images showed that HAP1 enhanced LC3 and LAMP1 puncta formation compared with the control experiments (Fig. 4D). In contrast, HAP1 was not co-localized with the endosome marker EEA1 (Fig. 4E), which suggested that HAP1 regulates autophagy without involving lysosome maturation.

3.5. HAP1 interacts with the PtdIns3K complex

Initiation of autophagy involves formation of isolation membranes known as phagophores. The process requires generation of PtdIns3P by class 3 phosphatidylinositol 3-kinase (PtdIns3K) complex containing BECN1, VPS34, VPS15 and ATG14 (Diao et al., 2015; Matsunaga et al., 2009; Zhong et al., 2009). We examined whether HAP1 can interact with the PtdIns3K complex. Exogenously expressed ATG14 was diffusely distributed in the cytoplasm of HeLa cells. In contrast, ATG14 adopted a punctate distribution and partially co-localized with HAP1 in cells co-expressing HAP1, the specific ATG14 puncta were clearly observed (Fig. 5A). VPS34, the catalytic subunit of the PtdIns3K complex, also showed diffused cytosolic distribution. HAP1 expression induced VPS34 puncta formation, albeit the puncta were much fewer in number than ATG14 puncta (Fig. 5B). Reciprocal co-immunoprecipitation verified the interaction between HAP1 and ATG14 (Fig. 5C). In contrast, HAP1 did not interact with UVAG, a PtdIns3K complex component that was involved in other autophagosome steps than initiation (Fig. 5E) (Itakura et al., 2008; Liang et al., 2008). These results further suggested that HAP1 mainly functions in autophagy initiation. We mapped the domain of HAP1 mediating its interaction with ATG14 to the coiled coil region (Fig. 5D), resembling the interaction between

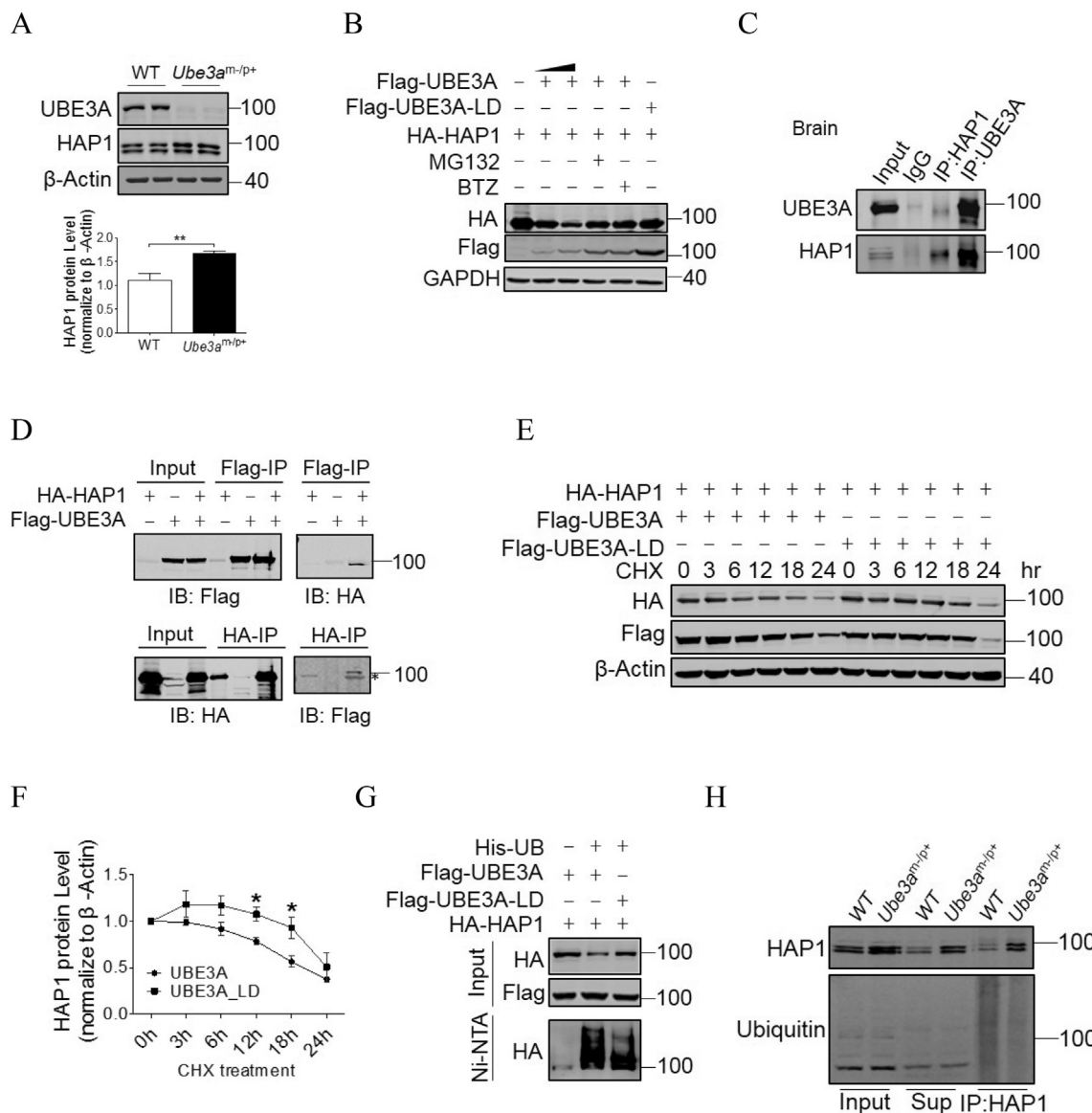


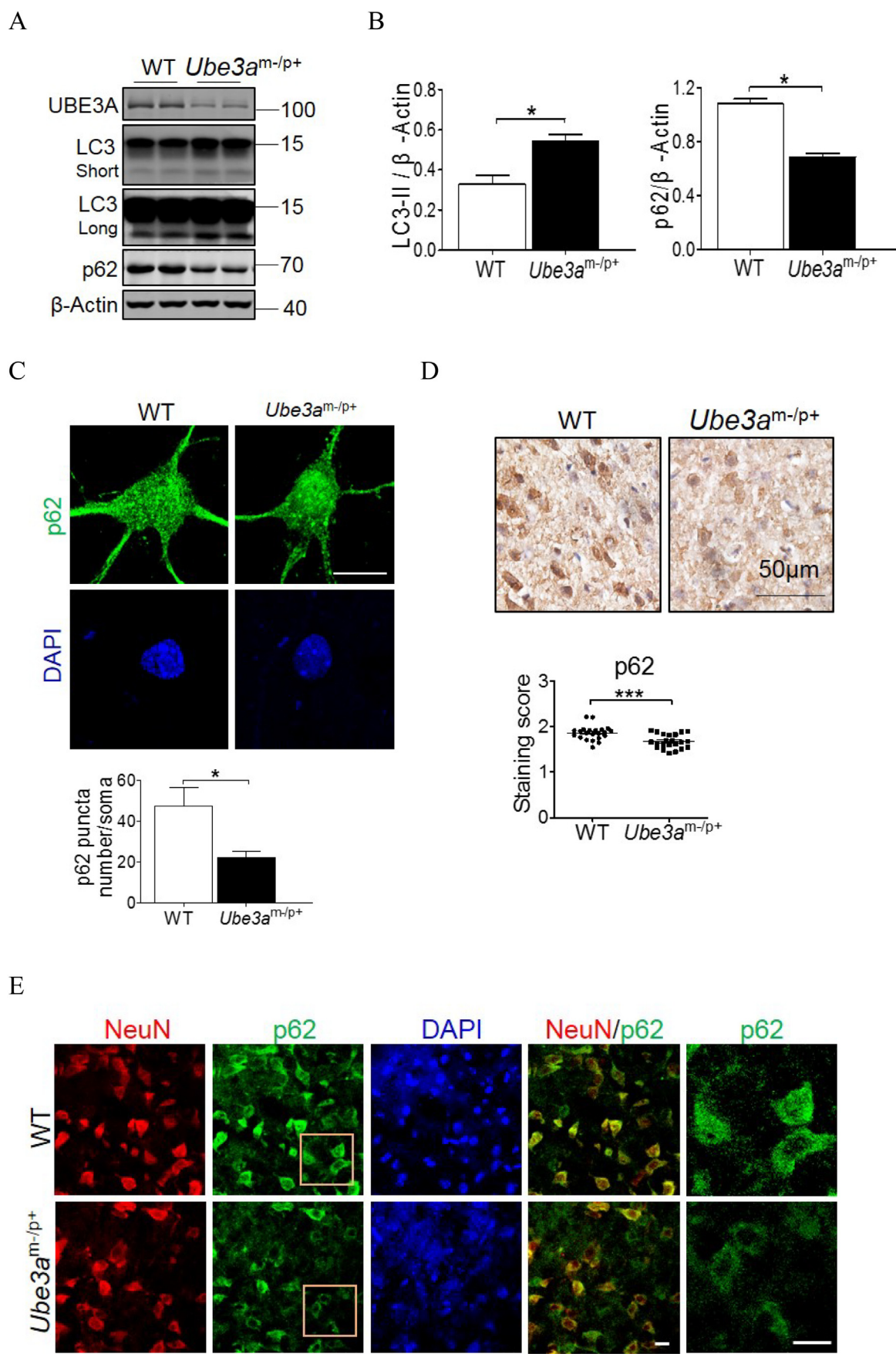
Fig. 2. HAP1 interacts with and is ubiquitinated by UBE3A. (A) HAP1 protein expression in P14 brain lysates were analyzed by western blot, and the bar graph shows quantitation of HAP1 levels. Error bars show SEM of 5 independent experiments. Student's t-test: **p < .01. (B) HEK293T cells were transfected with HAP1 and UBE3A (0.5 μg and 1.5 μg of DNA, respectively) or UBE3A-LD (Ligase dead), MG132 (10 μM) or BTZ (10 μM) was applied for 12 h. (C) Interaction between HAP1 and UBE3A in brain lysates at P14, IgG was used as a negative control. (D) HEK293T cells expressing Flag-UBE3A and HA-HAP1 were immunoprecipitated and detected by western blot. * Represents non-specific signal. (E-F) HAP1 stability in HEK293T cells co-transfected with UBE3A or UBE3A-LD, and the quantitative analysis was displayed in (F). Error bars show SEM of 5 independent experiments. Student's t-test: *p < .05. (G) Ubiquitylation of HAP1 in cells. HEK293T cells were co-transfected with HA-HAP1 and Flag-UBE3A, or HA-HAP1 and Flag-UBE3A-LD plasmids. Protein extracts were purified with Ni-NTA column and analyzed by western blot. (H) Ubiquitylation of HAP1 in P14 brain lysate from WT and AS mice. Endogenous HAP1 was immunoprecipitated followed by western blotting using an ubiquitin antibody.

ATG14 and BECN1 in the PtdIns3K complex (Li et al., 2012).

3.6. HAP1 regulates autophagy via promoting PtdIns3K complex formation

To examine whether HAP1 regulates PtdIns3K complex formation and activity, sucrose-gradient fractionation using mouse brain showed that HAP1 co-sedimented with the PtdIns3K complex (Fig. 6A). Similar experiments conducted in HEK293T cells showed that the major ATG14-VPS34-BECN1 peaks sedimented in higher sucrose concentration in HAP1-transfected cells, suggesting that HAP1 interacted with the PtdIns3K complex to form a larger complex (Fig. S4A). Gel filtration analysis using WT brain also detected a BECN1-VPS34 complex with a molecular weight between 440 and 670 KD that co-eluted with HAP1 (Fig. 6B). Moreover, overexpressing HAP1 increased the interaction

between ATG14 and BECN1 (Fig. 6C), potentially enhancing the complex formation. To further investigate whether HAP1 modulates the activity of PtdIns3K in vivo, we measured PtdIns3P production in cortical neurons at DIV12 using quantitative ELISA analysis. As expected, PtdIns3K activity increased significantly in AS neurons compared with WT neurons. Interestingly, reducing HAP1 expression by siRNA significantly alleviated the increased PtdIns3P production in AS neurons (Fig. 6D). Phosphorylation of BECN1 at serine 93 increased in AS brain and cortical neurons (Fig. 6E-F), further supporting an increased PtdIns3K activity (Kim et al., 2013). As the scaffolding protein of the PtdIns3K complex, BECN1 showed no direct interaction or localization with HAP1 (Fig. S4B-C). Collectively, our data demonstrate that in AS neurons the increased HAP1 levels enhanced PtdIns3K complex assembly and activity.



(caption on next page)

Fig. 3. Autophagy activity is increased in the brain and primary cortical neurons of AS mouse. (A-B) Autophagy level was measured in WT and AS cortical neurons at DIV12. Autophagy markers LC3 and p62 were monitored using specific antibodies. Statistical analysis of p62 and LC3 were shown in (B). Error bars display SEM of 4 independent experiments. Student's *t*-test: ***p* < .01, ****p* < .001. (C) Immunofluorescence imaging of endogenous p62 in cortical neurons after chloroquine treatment (20 μ M, 4 h), the number of puncta per neuronal soma were quantified. Student's *t*-test: **p* < .05, ***p* < .001, *n* = 15. Scale bar: 10 μ m. (D) Immunohistochemistry staining of p62 in cortical region of P14 mice. The brown cells were counted as positive cells. A total of four mice per genotype, and 6 brain slides per mouse were counted, and the staining scores were presented in mean \pm S.E.M. Student's *t*-test: ****p* < .001. (E) Fluorescence histochemistry for p62 and NeuN in cortex region of P14 mice. Scale bar: 10 μ m. (For interpretation of the references to colour in this figure legend, the reader is referred to the web version of this article.)

3.7. HAP1 participates in later stages of autophagosome formation and promotes autophagic flux

To assess whether HAP1 plays a role in later stages of autophagy, we

imaged cellular distribution of DFCP1 (Double FYVE-containing protein 1), an indicator of phagophore-associated, PtdIns3P-enriched membrane formation from the endoplasmic reticulum. In HAP1-expressing HeLa cells, there were increased DFCP1-labeled puncta (green),

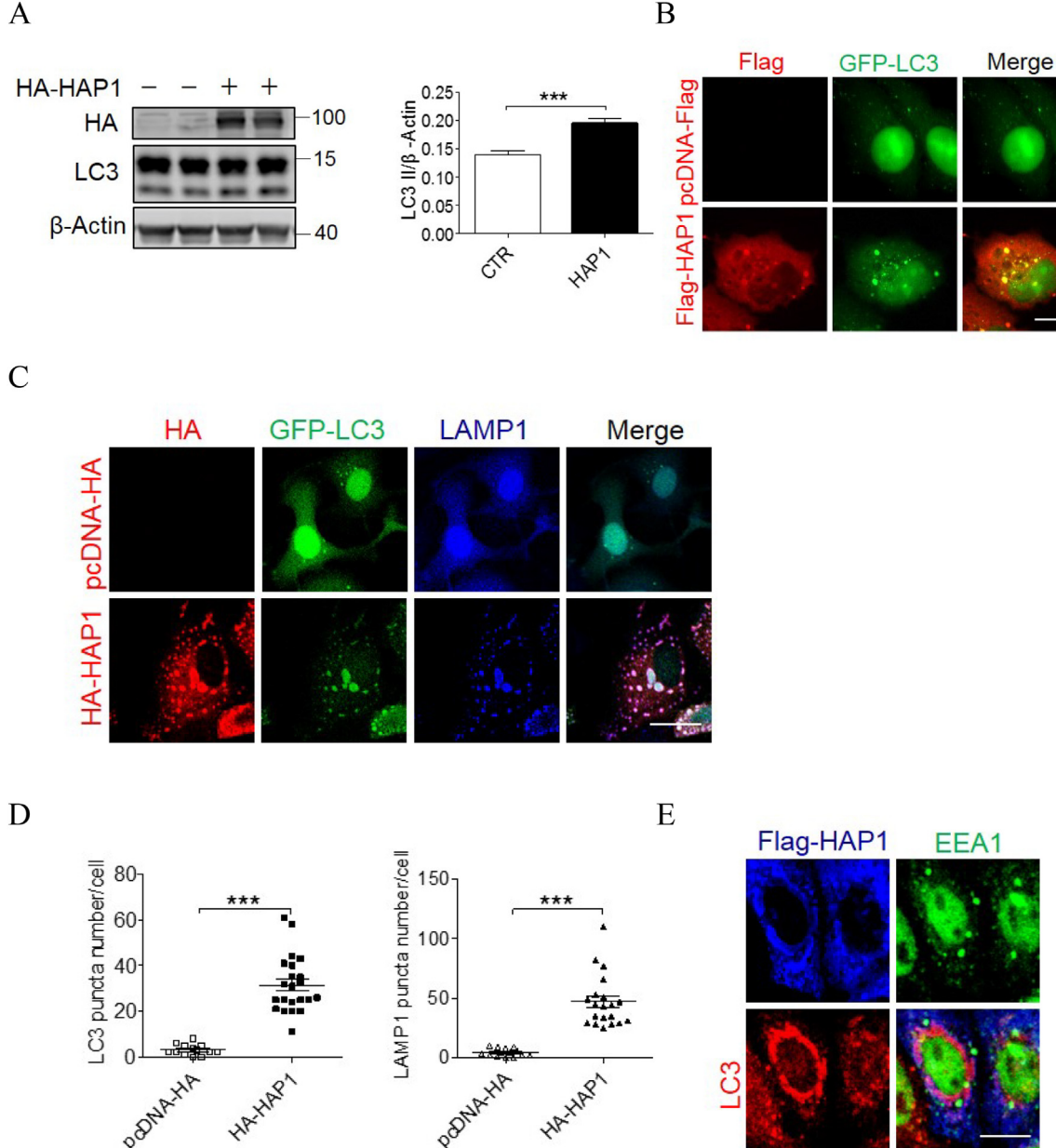
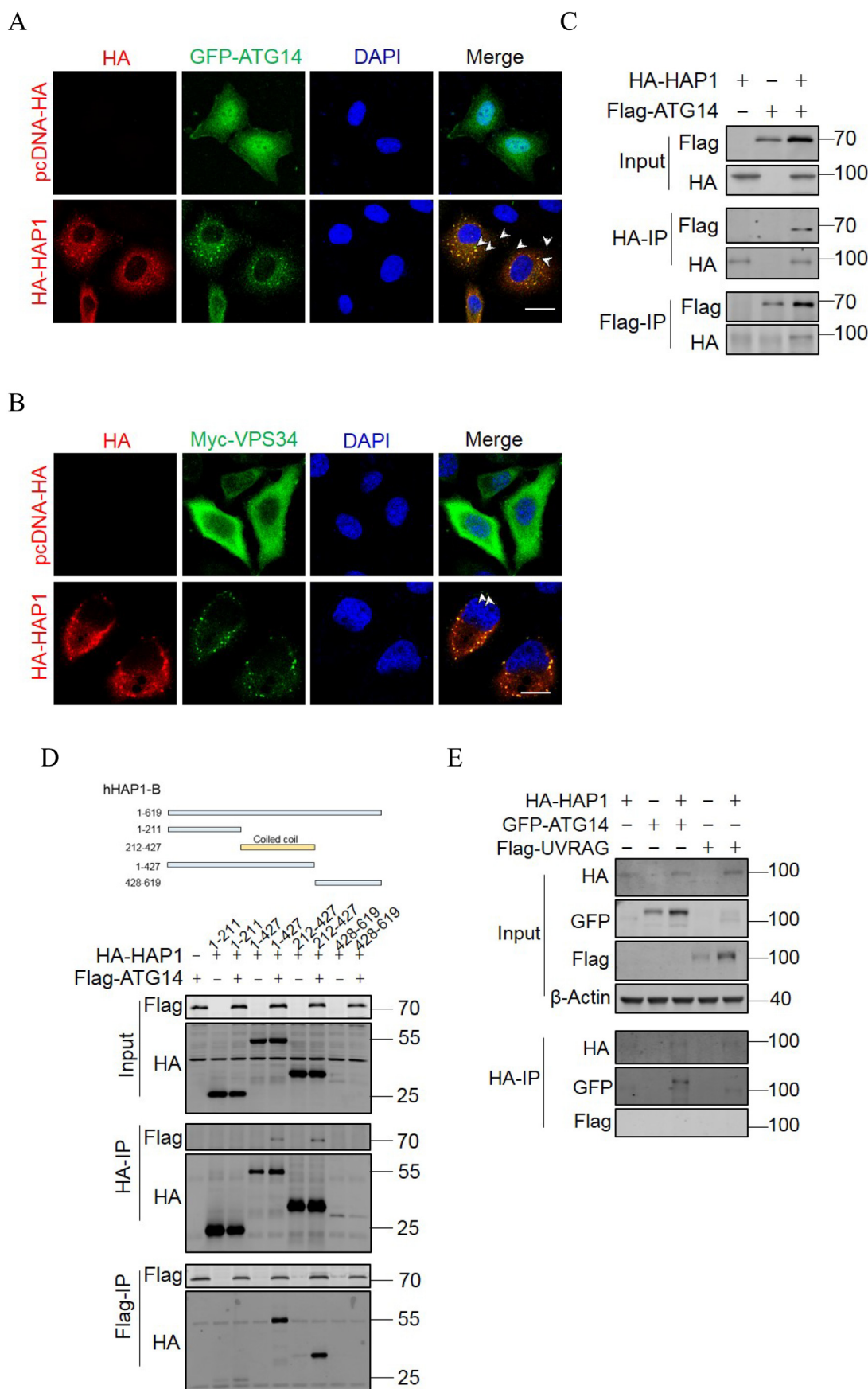


Fig. 4. HAP1 enhances basal autophagy. (A) HA-HAP1 was transfected into HEK293T cells and LC3 levels were measured using western blot. Error bars display SEM of 7 independent experiments. Student's *t*-test: ****p* < .001. (B) Flag-HAP1 was expressed in HeLa cells together with GFP-LC3, immunofluorescent imaging was used to measure HAP1 localization with LC3. Scale bar: 10 μ m. (C) HAP1 and GFP-LC3 were expressed in HeLa cells. The cells were immunofluorescent labeled with antibodies against HA (HAP1, red) and LAMP1 (blue), and imaged by confocal microscopy. Scales bar: 10 μ m. (D) LC3 or LAMP1 puncta number were quantified in HeLa transfected with pcDNA3.1 or HA-HAP1, respectively. Error bars show SEM of 20 transfected cells. Student's *t*-test: ****p* < .001. (E) Triple immunofluorescent labeling of flag-tagged HAP1 and endogenous LC3 and EEA1 in HeLa cells. Scales bar: 10 μ m. (For interpretation of the references to colour in this figure legend, the reader is referred to the web version of this article.)



(caption on next page)

Fig. 5. HAP1 interacts with the PtdIns3K complex. (A-B) Immunofluorescence imaging of HeLa cells co-transfected with HA-HAP1 and ATG14 or HA-HAP1 and VPS34. Scale bar: 10 μm. Arrows indicate specific ATG14 or VPS34 puncta. (C) HeLa cells expressing HA-HAP1 and Flag-ATG14 were immunoprecipitated and detected by western blot. (D) Truncation mutations of HAP1 were co-transfected with ATG14 in HEK293T cells, and were immunoprecipitated using the indicated antibodies and detected by western blot. (E) HeLa cells expressing HA-HAP1 and GFP-ATG14 or HA-HAP1 and Flag-UVRAG were immunoprecipitated and detected by western blot. ATG14 served as a positive control.

together with a large proportion of DFCP1 puncta co-localizing with HAP1 (red, Fig. 7A). WIPI2, another PtdIns3P binding protein, was diffusely distributed in the cytoplasm of HeLa cells when HAP1 was over expressed (Fig. S5A), suggesting that HAP1 has negligible effect on LC3 lipidation (Polson et al., 2010). Together, these results indicate that HAP1 promotes autophagosome formation primarily in early steps. We then performed autophagic flux assay in HeLa cells by monitoring the fluorescent signal of a tandem RFP-GFP-LC3 reporter. HAP1 markedly increased autophagy flux, as red puncta increased in HAP1-expressing cells even at the basal level. HAP1 enhancement of autophagic flux was even more dramatic after glucose starvation (Fig. 7B-D). When the acidic environment inside the lysosome was neutralized by CQ, both the control and HAP1-transfected cells showed stabilization of GFP signals and thus co-staining of red and green puncta (Fig. 7B-C). Collectively, HAP1 appears to promote autophagic flux by enhancing the initiation of autophagy and participating in autophagosome elongation.

3.8. Inhibiting autophagy rescues synaptic pathology and some behavioral abnormalities

Since dendritic spines in AS neurons display abnormal shape and reduced number (Dindot et al., 2008; Margolis et al., 2010), we asked whether exaggerated autophagy downstream of HAP1 could contribute to this type of spine abnormalities. We first tested whether the higher autophagy activity in AS neurons can be alleviated by reducing HAP1 expression. Knocking down HAP1 using siRNA in AS neurons reduced autophagy close to WT levels, as measured by LC3 expression (Fig. 8A-B). We then used a pharmacological approach to test whether inhibiting autophagy in AS neurons can rescue the abnormal dendritic spine morphology. Applying hydroxychloroquine (HCQ), a CQ derivative in clinical use that has less side effects (Costedoat-Chalumeau et al., 2015; Kroemer, 2015), to cortical neurons resulted in conversion of LC3 to LC3II and accumulation of p62 in a time dependent manner (Fig. 8C-D). We opted to use a longer treatment time (5 μM, 12 h) for dendritic spine analysis. At DIV 16, AS cortical neurons showed decreased dendritic

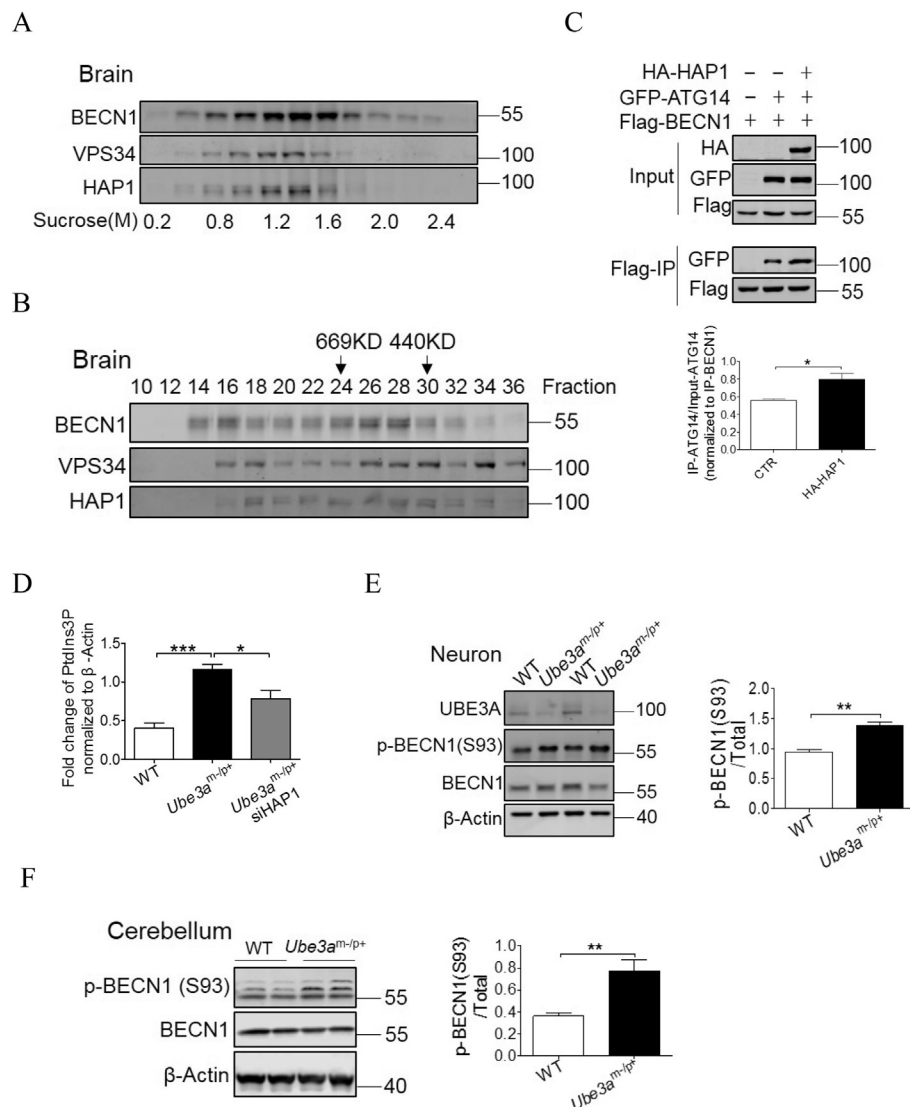


Fig. 6. HAP1 regulates autophagy by promoting PtdIns3K complex formation. (A) Sucrose density gradient centrifugation of P14 mouse brain lysate followed by western blot detection using antibodies against endogenous HAP1 and PtdIns3K complex components. The concentration of sucrose was from 0.2 M to 2.4 M. (B) The supernatants of brain lysates from WT mouse at P14 were subjected to gel filtration analysis, followed by WB. (C) HEK293T cells expressing Flag-BECN1, GFP-ATG14, with or without HA-HAP1 were immunoprecipitated using an anti-Flag antibody and detected using western blot. The GFP-ATG14 signal intensity was quantified and normalized to ATG14 signal from the input. (D) Cortical neurons at DIV12 were lysed and subjected to a quantitative PtdIns3P ELISA assay. Statistical analysis of PtdIns3P signal intensity normalized to β-actin was shown. Error bars indicated SEM of 5 independent experiments. Student's t-test: * $p < .05$, *** $p < .001$. (E) Phosphorylation of BECN1 at serine 93 was detected in WT and AS cortical neurons at DIV12 using a phosphorylation-specific antibody. Error bar displays SEM of 3 independent experiments Student's t-test: * $p < .05$. (F) Phosphorylation of BECN1 at serine 93 was detected using a phosphorylation-specific antibody in cerebellum region at P14, both the two bottom bands were positive signal and used for the quantification.

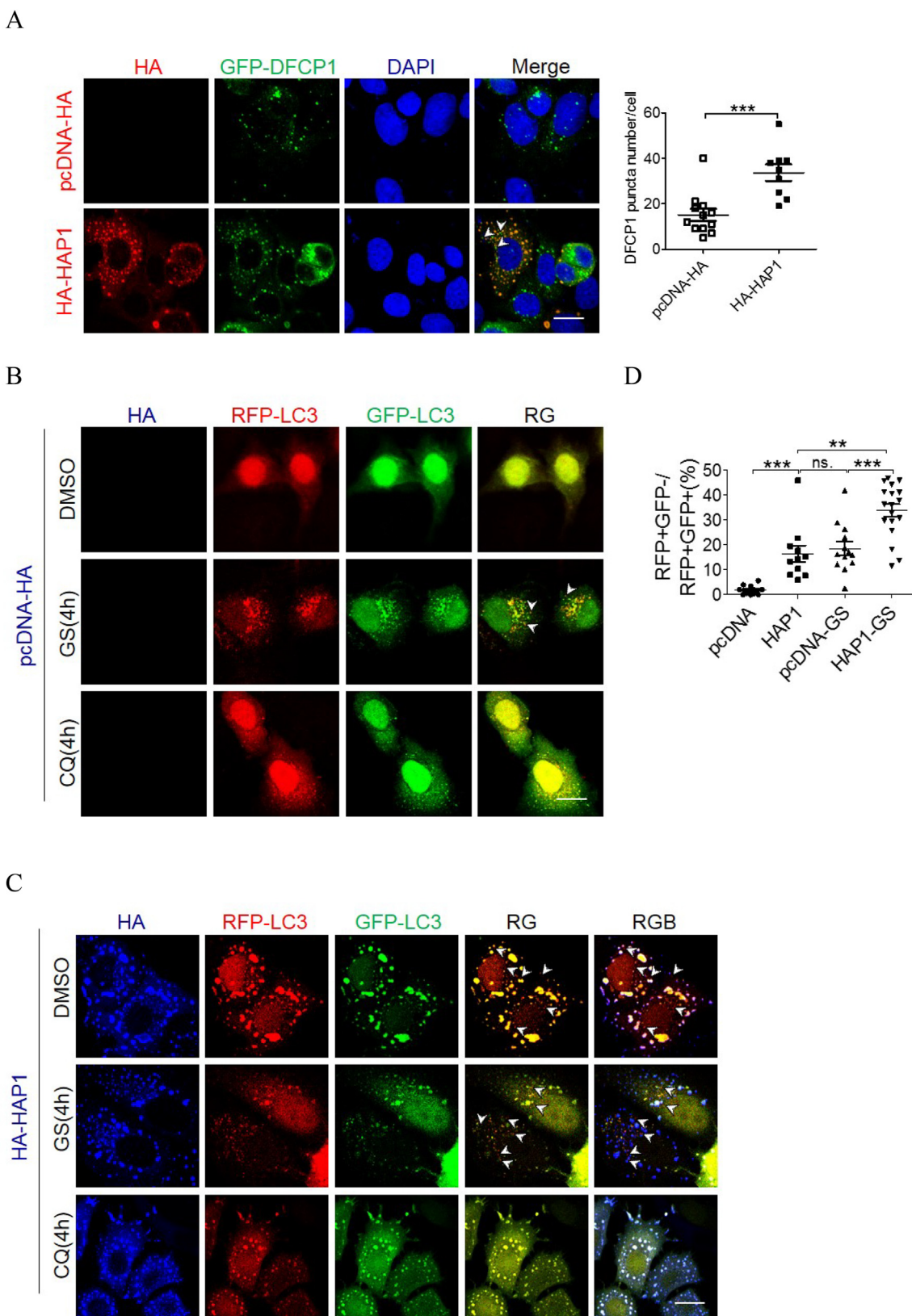


Fig. 7. HAP1 localizes in later stages of autophagosome. (A) HA-HAP1 and GFP-DFCP1 were expressed in HeLa cells followed by immunofluorescent labeling and confocal microscopy imaging. HAP1: red, DFCP1: green, scale bar: 10 μ m. Arrows indicate specific DFCP1 puncta. The DFCP1 puncta number was quantified ($n = 9$). *** $P < .001$. (B-C) RFP-GFP-LC3 was expressed with HA-HAP1 or pcDNA-HA plasmid in HeLa cells, respectively. Cells were glucose starved for 4 h or treated with chloroquine (20 μ M, 4 h), and LC3 was monitored by fluorescence confocal microscope. Scale bar: 10 μ m. GFP-negative and RFP-positive puncta indicate autophagic flux. Arrows indicate specific red signal representing lysosome. (D) Error bars indicate SEM of independent experiments ** $p < .01$, *** $p < .001$, $n = 15$ cells. (For interpretation of the references to colour in this figure legend, the reader is referred to the web version of this article.)

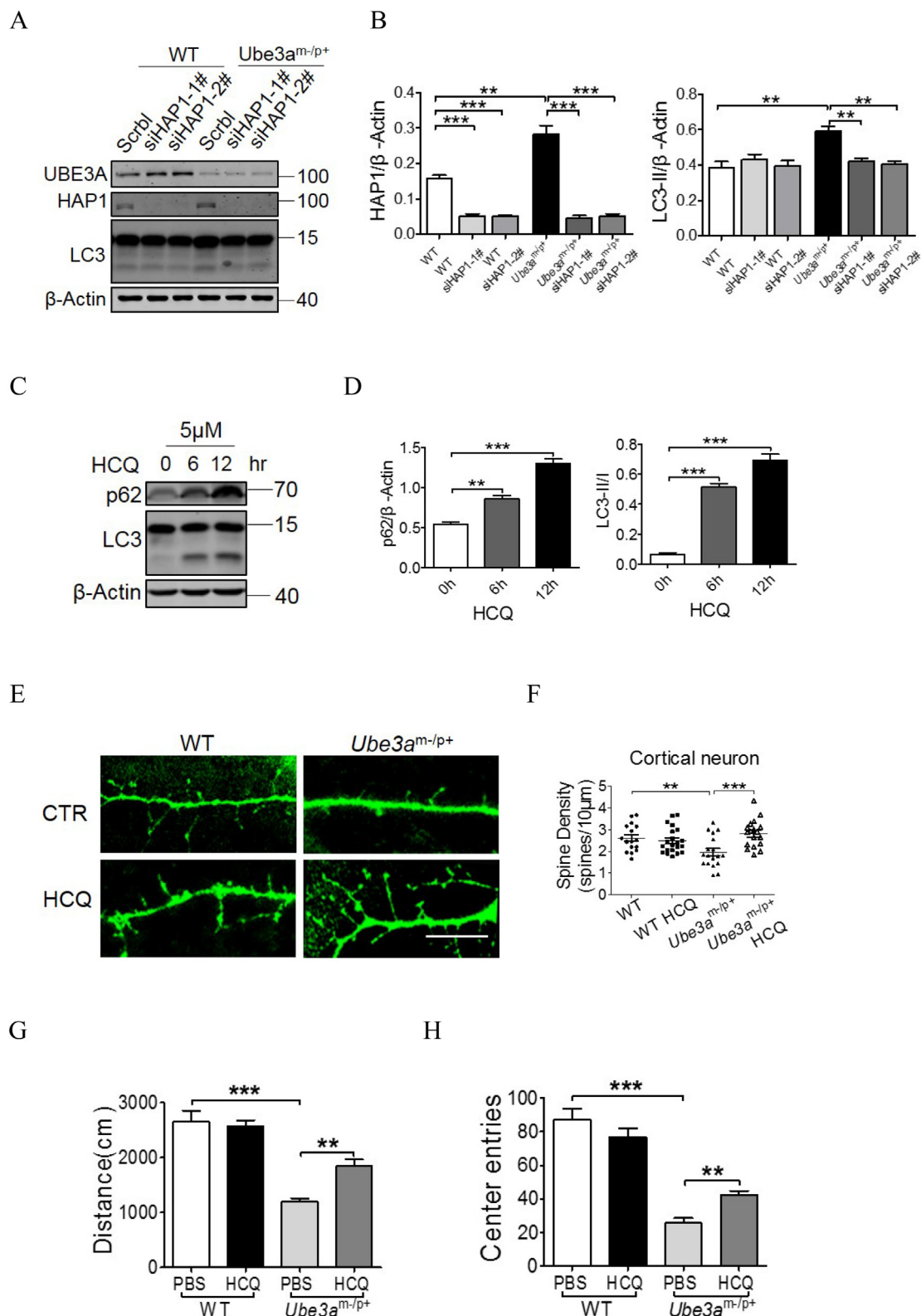


Fig. 8. Inhibiting autophagy rescues synaptic spine abnormality in AS neurons. (A) AS cortical neurons were transfected with scramble siRNA (Scrbl) or HAP1 siRNA at DIV10, neurons were collected 2 days later for western blot analysis using antibodies against HAP1 and LC3. (B) Bar graph shows the expression of HAP1 and LC3II normalized to β -Actin. Error bars indicated SEM of 4 independent experiments. Student's t-test: ** $p < .01$, *** $p < .001$. (C-D) Cortical neurons at DIV16 were treated with hydroxychloroquine (HCQ) at various time points, followed by western blot analysis using antibodies against p62 and LC3. Error bars indicated SEM of 4 independent experiments. Student's t-test: ** $p < .01$, *** $p < .001$. (E) Representative images of dendritic spines of DIV 16 cortical neurons infected with Lenti-GFP. Neurons were fixed for fluorescence confocal microscopy analysis. HCQ: 5 μ M, 12 h, scale bar: 10 μ m. (F) Statistical analysis of spine density from 18 neurons per condition. Error bars represent SEM, Student's t-test: ** $p < .01$, *** $p < .001$. (G) Open field test was performed at P30 after inhibiting autophagy with HCQ every 2 days starting from P14. Total distance traveled (G) and center entries (H) were collected and analyzed. Error bars represent SEM, Student's t-test: ** $p < .01$, *** $p < .001$, $n = 5$.

number comparing to WT neurons. After treating AS neurons with HCQ, there was a significantly increased spine density in the treated neurons compared to AS neurons without treatment (Fig. 8E-F).

We further tested whether inhibiting autophagy was able to rescue behavioral abnormalities in AS mice, including fear conditioning, rotarod and open field tests. Among these tests, performance in the open field showed promising improvement; comparing to AS mice injected with PBS, AS mice treated with HCQ traveled longer distance and are more prone to the center (Fig. 8G-H). However, deficits in freezing response to shock in the cued test and the contextual test, as well as rotarod test failed to show signs of alleviation (Fig. S6A-C).

4. Discussion

Given the ubiquitin ligase activity of UBE3A and its potentially large substrate pool, identifying its new targets in the context of the in vivo environment is important, particularly within the brain proteome. Our SILAM strategy meets this goal and identified potential new targets, on top of detecting a handful of known targets. Among the potential targets, we chose HAP1 for further biochemical and functional characterization. Our analysis shows that UBE3A controls the stability of HAP1 in the brain. In neurons with UBE3A insufficiency, HAP1 is aberrantly over expressed. HAP1 regulates autophagy at multiple steps, primarily by interacting with members of PtdIns3K complex ATG14 and VPS34, to increase the lipid kinase activity of PtdIns3K. Previous studies had demonstrated other proteins as key components in ATG14-containing PtdIns3K complex (Ma et al., 2014; Zhao et al., 2015), and our study provides new insight on the role of autophagy regulation in the context of Angelman syndrome. HAP1 is also involved in recruitment of proteins with PtdIns3P binding domains including DFCP1 to facilitate autophagosome formation. As a consequence, autophagy flux is enhanced. Collectively, we identified a neuronal UBE3A target that plays an important role in synaptic development via modulating autophagic activity.

To understand how UBE3A regulates HAP1 protein expression, we performed various experiments including protein-protein interaction, co-localization, protein stability and ubiquitination assays in cell lines and brain tissues. All evidence point to the conclusion that UBE3A regulates HAP1 expression at the protein level. Indeed, HAP1 ubiquitination depended on intact UBE3A activity. However, in vitro ubiquitination assay using purified proteins have not been successful in our hands, in spite of positive results using known UBE3A substrate HHR23A (Jiang et al., 1998) and UBE3A itself (data not shown). We therefore speculate that for HAP1 to become ubiquinated in a UBE3A-dependent manner, an unknown co-factor may be needed that was not supplied in vitro. Other posttranslational modifications, such as phosphorylation or sumoylation, may regulate ubiquitination of HAP1 in a sequential manner in vivo, which are missing under in vitro environment (Boutell et al., 2003; Hicke et al., 1998; Swaney et al., 2013). Alternatively, HAP1 may not be a direct target of UBE3A. Since UBE3A regulates HAP1 stability in a ligase-dependent manner and influences its ubiquitination level, it is possible that more intricate protein-protein interaction existed to indirectly influence HAP1 protein level through ubiquitin-proteasome pathway, and this type of indirect regulation has been demonstrated in other scenarios (Ferguson et al., 2013; Tsai et al., 2012). Nevertheless, our data point to the parsimonious conclusion that HAP1 is regulated by UBE3A at protein level.

Deregulated autophagic degradation of protein aggregates and damaged organelles have been associated with a variety of disorders, particularly neurodegeneration and neurodevelopmental disorders (Cuervo et al., 2004; Lee et al., 2010; Ravikumar et al., 2004). Synaptic pruning defects leading to increased spine density has been associated with reduced autophagy (Tang et al., 2014; Yan et al., 2018). Our study is the first to establish the causal relationship between excessive autophagy and loss of spines in an AS mouse model. Furthermore, we identify a downstream UBE3A target that might be the culprit for the

excessive autophagy. In an autistic spectrum disorder that was caused by increased gene dosage of UBE3A, spine density was increased (Yi et al., 2015). Thus, it appears that autophagy might contribute to synaptic pruning in a bi-phasic manner, further highlighting the importance of autophagy in synaptic development. Deviations in the normal rate of autophagy during development by increased dosage effect of HAP1 may be a key determinant of synaptic dysfunction. From the perspective of autophagy regulation, our findings provide a new avenue to understand the structural abnormalities occurred in dendritic spines in AS neurons.

Because the loss of UBE3A leads to multiple behavioral abnormalities in patients, UBE3A must regulate CNS wiring and development through an intricate network of targets. Our pharmacological approach using an autophagy inhibitor results in at least partial rescue of abnormalities in open field test, while other behavioral deficits failed to show signs of alleviation. Nevertheless, we believe that reducing autophagic activity directly or through knocking down HAP1 expression has the potential to improve at least some of the behavioral deficits. Further optimization of administration strategies or selection of compounds that are more potent and more permeable to blood-brain barrier is needed. Furthermore, as AS mouse has a distinct development window (Silva-Santos et al., 2015), proper treatment time window and treatment duration might also be crucial. Future studies attempting to rescue deficits in dendritic spine density in vivo, as well as to rescue behavioral deficits through modulating autophagy, will be important extensions to this study.

Supplementary data to this article can be found online at <https://doi.org/10.1016/j.nbd.2019.104585>.

Author contributions

T.W., X.L., Z.X. and L.L. designed the research; T.W., J.W., J.W., L.M., Y.Z., and L.L. performed research; B.T., T.W. and L.L. analyzed data; and T.W., P.W.V., and L.L. wrote the paper.

Declaration of Competing Interest

The authors declare no conflict of interest for this study.

Note: Raw mass spectrometry data is available in PXD013624 and PXD013625.

Acknowledgements

The authors would like to acknowledge financial support from East China Normal University (ECNU) National "985" Project grant (No. 11300-120215-10463) from China to LL.

The authors also acknowledge support of animal experiments from ECNU Multifunctional Platform for Innovation (011).

References

- Boutell, C., Orr, A., Everett, R.D., 2003. PML residue lysine 160 Is required for the degradation of PML induced by Herpes Simplex Virus Type 1 Regulatory Protein ICP0. *J. Virol.* 77, 8686–8694.
- Costedoat-Chalumeau, N., Dunogué, B., Leroux, G., Morel, N., Jallouli, M., Le Guern, V., Piette, J.-C., Brézin, A.P., Melles, R.B., Marmor, M.F., 2015. A critical review of the effects of hydroxychloroquine and chloroquine on the eye. *Clin. Rev. Allergy Immunol.* 49, 317–326.
- Cuervo, A.M., Stefanis, L., Fredenburg, R., Lansbury, P.T., Sulzer, D., 2004. Impaired degradation of mutant α -synuclein by chaperone-mediated autophagy. *Science* 305, 1292.
- de Bie, P., Ciechanover, A., 2011. Ubiquitination of E3 ligases: self-regulation of the ubiquitin system via proteolytic and non-proteolytic mechanisms. *Cell Death Differ.* 18, 1393–1402.
- Diao, J., Liu, R., Rong, Y., Zhao, M., Zhang, J., Lai, Y., Zhou, Q., Wilz, L.M., Li, J., Vivona, S., et al., 2015. ATG14 promotes membrane tethering and fusion of autophagosomes to endolysosomes. *Nature* 520, 563–566.
- Dindot, S.V., Antalffy, B.A., Bhattacharjee, M.B., Beaudet, A.L., 2008. The Angelman syndrome ubiquitin ligase localizes to the synapse and nucleus, and maternal deficiency results in abnormal dendritic spine morphology. *Hum. Mol. Genet.* 17,

- 111–118.
- Engelender, S., Sharp, A.H., Colomer, V., Tokito, M.K., Lanahan, A., Worley, P., Holzbaur, E.L.F., Ross, C.A., 1997. Huntingtin-associated Protein 1 (HAP1) Interacts with the p150Glued Bubunit of Dynactin. *Hum. Mol. Genet.* 6, 2205.
- Ferguson, J.L., Chao, W.C.H., Lee, E., Friedman, K.L., 2013. The anaphase promoting complex contributes to the degradation of the *S. cerevisiae* telomerase recruitment subunit Est1p. *PLoS One* 8, e50555.
- Glessner, J.T., Wang, K., Cai, G., Korvatska, O., Kim, C.E., Wood, S., Zhang, H., Estes, A., Brune, C.W., Bradfield, J.P., et al., 2009. Autism genome-wide copy number variation reveals ubiquitin and neuronal genes. *Nature* 459, 569–573.
- Greer, P.L., Hanayama, R., Bloodgood, B.L., Mardinly, A.R., Lipton, D.M., Flavell, S.W., Kim, T.-K., Griffith, E.C., Waldon, Z., Maeahr, R., et al., 2010. The Angelman Syndrome-associated ubiquitin ligase Ube3A regulates synapse development by ubiquitinating Arc. *Cell* 140, 704–716.
- Gutekunst, C.-A., Li, S.-H., Yi, H., Ferrante, R.J., Li, X.-J., Hersch, S.M., 1998. The cellular and subcellular localization of Huntingtin-Associated Protein 1 (HAP1): comparison with huntingtin in rat and human. *J. Neurosci.* 18, 7674.
- Hicke, L., Zanolari, B., Riezman, H., 1998. Cytoplasmic tail phosphorylation of the α -factor receptor is required for its ubiquitination and internalization. *J. Cell Biol.* 141, 349–358.
- Hirokawa, N., 1998. Kinesin and dynein superfamily proteins and the mechanism of organelle transport. *Science* 279, 519.
- Itakura, E., Kishi, C., Inoue, K., Mizushima, N., 2008. Beclin 1 forms two distinct phosphatidylinositol 3-kinase complexes with mammalian Atg14 and UVRAG. *Mol. Biol. Cell* 19, 5360–5372.
- Jiang, Y.-H., Armstrong, D., Albrecht, U., Atkins, C.M., Noebels, J.L., Eichele, G., Sweat, J.D., Beaudet, A.L., 1998. Mutation of the angelman ubiquitin ligase in mice causes increased cytoplasmic p53 and deficits of contextual learning and long-term potentiation. *Neuron* 21, 799–811.
- Kim, J., Kim, Y.C., Fang, C., Russell, R.C., Kim, J.H., Fan, W., Liu, R., Zhong, Q., Guan, K.-L., 2013. Differential regulation of distinct Vps34 complexes by AMPK in nutrient stress and autophagy. *Cell* 152, 290–303.
- Kishino, T., Lalande, M., Wagstaff, J., 1997. UBE3A/E6-AP mutations cause Angelman syndrome. *Nat. Genet.* 15, 70.
- Kroemer, G., 2015. Autophagy: a druggable process that is deregulated in aging and human disease. *J. Clin. Invest.* 125, 1–4.
- Kühnle, S., Kogel, U., Glockzin, S., Marquardt, A., Ciechanover, A., Matentzoglu, K., Scheffner, M., 2011. Physical and functional interaction of the HECT ubiquitin-protein ligases E6AP and HERC2. *J. Biol. Chem.* 286, 19410–19416.
- Kühnle, S., Mothes, B., Matentzoglu, K., Scheffner, M., 2013. Role of the ubiquitin ligase E6AP/UBE3A in controlling levels of the synaptic protein Arc. *Proc. Natl. Acad. Sci. U. S. A.* 110, 8888–8893.
- Lee, J.-H., Yu, W.H., Kumar, A., Lee, S., Mohan, P.S., Peterhoff, C.M., Wolfe, D.M., Martínez-Vicente, M., Massey, A.C., Sovak, G., et al., 2010. Lysosomal proteolysis and autophagy require presenilin 1 and are disrupted by alzheimer-related PS1 mutations. *Cell* 141, 1146–1158.
- Li, X.-J., Li, S.-H., Sharp, A.H., Nucifora, F.C., Schilling, G., Lanahan, A., Worley, P., Snyder, S.H., Ross, C.A., 1995. A huntingtin-associated protein enriched in brain with implications for pathology. *Nature* 378, 398.
- Li, S.-H., Gutekunst, C.-A., Hersch, S.M., Li, X.-J., 1998. Interaction of huntingtin-associated protein with dynactin P150 $<\sup>$ Glued $</sup>$. *J. Neurosci.* 18, 1261.
- Li, X., He, L., Zhang, M., Yue, Z., Zhao, Y., 2012. The BECN1 coiled coil domain: An “imperfect” homodimer interface that facilitates ATG14 and UVRAG binding. *Autophagy* 8, 1258–1260.
- Li, J., Kim, S.G., Blenis, J., 2014. Rapamycin: one drug, many effects. *Cell Metab.* 19, 373–379.
- Liang, C., Lee, J.S., Inn, K.-S., Gack, M.U., Li, Q., Roberts, E.A., Vergne, I., Deretic, V., Feng, P., Akazawa, C., et al., 2008. Beclin1-binding UVRAG targets the class C Vps complex to coordinate autophagosome maturation and endocytic trafficking. *Nat. Cell Biol.* 10, 776–787.
- Ma, B., Cao, W., Li, W., Gao, C., Qi, Z., Zhao, Y., Du, J., Xue, H., Peng, J., Wen, J., et al., 2014. Dapper1 promotes autophagy by enhancing the Beclin1-Vps34-Atg14L complex formation. *Cell Res.* 24, 912–924.
- Mabb, A.M., Judson, M.C., Zylka, M.J., Philpot, B.D., 2011. Angelman syndrome: insights into genomic imprinting and neurodevelopmental phenotypes. *Trends Neurosci.* 34, 293–303.
- Margolis, S.S., Salogiannis, J., Lipton, D.M., Mandel-Brehm, C., Wills, Z.P., Mardinly, A.R., Hu, L., Greer, P.L., Bikoff, J.B., Ho, H.-Y.H., et al., 2010. EphB-mediated degradation of the RhoA GEF Ephexin5 relieves a developmental brake on excitatory synapse formation. *Cell* 143, 442–455.
- Martinez-Zapien, D., Ruiz, F.X., Poirson, J., Mitschler, A., Ramirez-Ramos, J., Forster, A., Cousido-Siah, A., Masson, M., Pol, S.V., Podjarny, A., et al., 2016. Structure of the E6/E6AP/p53 complex required for HPV-mediated degradation of p53. *Nature* 529, 541–545.
- Matsunaga, K., Saitoh, T., Tabata, K., Omori, H., Satoh, T., Kurotori, N., Maejima, I., Shirahama-Noda, K., Ichimura, T., Isobe, T., et al., 2009. Two Beclin 1-binding proteins, Atg14L and Rubicon, reciprocally regulate autophagy at different stages. *Nat. Cell Biol.* 11, 385.
- Mejia, L.A., Litterman, N., Ikeuchi, Y., de la Torre-Ubieta, L., Bennett, E.J., Zhang, C., Harper, J.W., Bonni, A., 2013. A Novel Hap1-Tsc1 interaction regulates neuronal mTORC1 signaling and morphogenesis in the brain. *J. Neurosci.* 33, 18015–18021.
- Pastuzyn, E.D., Shepherd, J.D., 2017. Activity-dependent arc expression and homeostatic synaptic plasticity are altered in neurons from a mouse model of Angelman syndrome. *Front. Mol. Neurosci.* 10, 234.
- Polson, H.E.J., de Lartigue, J., Rigden, D.J., Reedijk, M., Urbé, S., Clague, M.J., Tooze, S.A., 2010. Mammalian Atg18 (WIP12) localizes to omegasome-anchored phagophores and positively regulates LC3 lipidation. *Autophagy* 6, 506–522.
- Ravikumar, B., Vacher, C., Berger, Z., Davies, J.E., Luo, S., Orosz, L.G., Scaravilli, F., Easton, D.F., Duden, R., O'Kane, C.J., et al., 2004. Inhibition of mTOR induces autophagy and reduces toxicity of polyglutamine expansions in fly and mouse models of Huntington disease. *Nat. Genet.* 36, 585.
- Rong, J., Li, S.-H., Li, X.-J., 2007. Regulation of intracellular HAP1 trafficking. *J. Neurosci. Res.* 85, 3025–3029.
- Silva-Santos, S., van Woerden, G.M., Bruinsma, C.F., Mientjes, E., Jolfaei, M.A., Distel, B., Kushner, S.A., Elgersma, Y., 2015. Ube3a reinstatement identifies distinct developmental windows in a murine Angelman syndrome model. *J. Clin. Invest.* 125, 2069–2076.
- Su, L.-Y., Luo, R., Liu, Q., Su, J.-R., Yang, L.-X., Ding, Y.-Q., Xu, L., Yao, Y.-G., 2017. Atg5- and Atg7-dependent autophagy in dopaminergic neurons regulates cellular and behavioral responses to morphine. *Autophagy* 13, 1496–1511.
- Swaney, D.L., Beltrao, P., Starita, L., Guo, A., Rush, J., Fields, S., Krogan, N.J., Villén, J., 2013. Global analysis of phosphorylation and ubiquitylation crosstalk in protein degradation. *Nat. Methods* 10. <https://doi.org/10.1038/nmeth.2519>.
- Tang, G., Gudsnuk, K., Kuo, S.-H., Cotrina, M.L., Rosoklja, G., Sosunov, A., Sonders, M.S., Kanter, E., Castagna, C., Yamamoto, A., et al., 2014. Loss of mTOR-dependent macroautophagy causes autistic-like synaptic pruning deficits. *Neuron* 83, 1131–1143.
- Tang, B., Wang, T., Wan, H., Han, L., Qin, X., Zhang, Y., Wang, J., Yu, C., Berton, F., Francesconi, W., et al., 2015. Fmr1 deficiency promotes age-dependent alterations in the cortical synaptic proteome. *Proc. Natl. Acad. Sci. U. S. A.* 112, E4697–E4706.
- Tsai, N.-P., Wilkerson, J.R., Guo, W., Makinsonova, M.A., DeMartino, G.N., Cowan, C.W., Huber, K.M., 2012. Multiple autism-linked genes mediate synapse elimination via proteasomal degradation of a synaptic scaffold PSD-95. *Cell* 151, 1581–1594.
- Twelvetrees, A.E., Yuen, E.Y., Arancibia-Carcamo, I.L., MacAskill, A.F., Rostaing, P., Lumb, M.J., Humbert, S., Triller, A., Saudou, F., Yan, Z., et al., 2010. Deslivery of GABA(A)Rs to synapses is mediated by HAP1-KIF5 and disrupted by mutant huntingtin. *Neuron* 65, 53–65.
- Wang, Y., Liu, X., Zhou, L., Duong, D., Bhuripanyo, K., Zhao, B., Zhou, H., Liu, R., Bi, Y., Kiyokawa, H., et al., 2017. Identifying the ubiquitination targets of E6AP by orthogonal ubiquitin transfer. *Nat. Commun.* 8, 2232.
- Wong, Y.C., Holzbaur, E.L.F., 2014. The regulation of autophagosome dynamics by huntingtin and HAP1 is disrupted by expression of mutant huntingtin, leading to defective cargo degradation. *J. Neurosci.* 34, 1293–1305.
- Xiang, J., Yan, S., Li, S.-H., Li, X.-J., 2015. Postnatal loss of Hap1 reduces hippocampal neurogenesis and causes adult depressive-like behavior in mice. *PLoS Genet.* 11, e1005175.
- Yan, J., Porch, M.W., Court-Vazquez, B., Bennett, M.V.L., Zukin, R.S., 2018. Activation of autophagy rescues synaptic and cognitive deficits in fragile X mice. *Proc. Natl. Acad. Sci. U. S. A.* 115, E9707.
- Yang, Y., Coleman, M., Zhang, L., Zheng, X., Yue, Z., 2013. Autophagy in axonal and dendritic degeneration. *Trends Neurosci.* 36, 418–428.
- Yi, J.J., Berrios, J., Newbern, J.M., Snider, W.D., Philpot, B.D., Hahn, K.M., Zylka, M.J., 2015. An autism-linked mutation disables phosphorylation control of UBE3A. *Cell* 162, 795–807.
- Zhao, Y., Wang, Q., Qiu, G., Zhou, S., Jing, Z., Wang, J., Wang, W., Cao, J., Han, K., Cheng, Q., et al., 2015. RACK1 promotes autophagy by enhancing the Atg14L-Beclin 1-Vps34-Vps15 complex formation upon phosphorylation by AMPK. *Cell Rep.* 13, 1407–1417.
- Zhong, Y., Wang, Q.J., Li, X., Yan, Y., Backer, J.M., Chait, B.T., Heintz, N., Yue, Z., 2009. Distinct regulation of autophagic activity by Atg14L and Rubicon associated with Beclin 1-phosphatidylinositol 3-kinase complex. *Nat. Cell Biol.* 11, 468–476.